Progress In Electromagnetics Research, Vol. 142, 353–368, 2013

A DISPERSIVE CONFORMAL FDTD TECHNIQUE FOR ACCURATE MODELING ELECTROMAGNETIC SCATTERING OF THZ WAVES BY INHOMOGENEOUS PLASMA CYLINDER ARRAY

Xia Ai[1, *], Yuan Tian[2], Zhi Wei Cui[2], Yi Ping Han[2], and Xiao Wei Shi[1]

[1]National Laboratory of Science and Technology on Antennas and Microwaves, Xidian University, Xi'an, Shaanxi 710071, China

[2]School of Science, Xidian University, Xi'an, Shaanxi 710071, China

Abstract—A dispersive conformal FDTD method has been proposed to accurately model the interface between two adjacent dispersive mediums and implemented to study the scattering of THz electromagnetic (EM) waves by inhomogeneous collisional plasma cylinder array. The method is based on the technology of area average, which is different from existing dispersive conformal FDTD schemes. Numerical results show that the proposed method enhances the accuracy level compared to the staircasing FDTD scheme involved in the inhomogeneous plasma. It is interesting to find that the THz EM waves can propagate through the plasma array more easily with higher frequencies or larger separations, hence the scattering width in the backward direction becomes smaller, and the forward scattering exhibits a little different. This study will be useful for further designing intelligent plasma antenna arrays in the THz band and terahertz reentry telemetry through plasma.

1. INTRODUCTION

Over the past decades, the interaction of the electromagnetic (EM) wave with plasma has drawn great attention of many researchers in studies of radio telemetry of reentry bodies [1–3] and intelligent plasma antenna design [4–8]. Nevertheless, almost all these researches were limited in the microwave frequency band. Since major technical

Received 24 May 2013, Accepted 10 August 2013, Scheduled 6 September 2013

* Corresponding author: Xia Ai (xai@mail.xidian.edu.cn).

advances in the developing of terahertz sources have been provided recently [9–12], several experimental and numerical works involved in the interaction between terahertz waves and plasmas have been reported [13–17]. All these previous works mainly focused on experiments or theoretical analysis of the propagation characteristics of EM wave in the plasma, and few scattering characteristics have been considered in these works. In addition, all the plasmas addressed in previous papers are single plasma object. Terahertz scattering characteristics of multiple plasma objects have not been presented, which will be useful in the future research concern with designing intelligent plasma antenna array [6, 7]. In our work, the scattering of multiple plasma columns illuminated by terahertz EM waves is investigated by finite difference time domain (FDTD) method.

The FDTD method [18–20] as a powerful and robust tool has been applied in solving various EM problems, including those concerned with frequency dispersive and non-dispersive materials due to its simplicity and accuracy. In order to model plasma materials, the dispersive FDTD method [21–25] should be used. However, the staircasing procedure would introduce significant errors when modeling objects with curved surfaces. Therefore, several efficient conformal techniques have been proposed to model curved dielectric surfaces so as to reduce staircasing errors [26–30]. However, these techniques were mainly related to the non-dispersive FDTD methods, and applications in dispersive FDTD methods have not attracted sufficient attention. In [31–33], a dispersive contour-path FDTD method was proposed. Nevertheless, this method could only deal with a single metal-dielectric interface. The curved surface in inhomogeneous plasma cylinder array exists not only at the plasma-vacuum interface, but also inside every inhomogeneous plasma cylinder in the array. Consequently, a conformal FDTD method for curved surface between two adjacent dispersive materials is necessary to ensure that one can accurately model the inhomogeneous plasma cylinder array.

In this paper, a conformal FDTD method for dispersive material is proposed to accurately model the scattering of inhomogeneous plasma cylinder array illuminated by terahertz EM waves. The effective permittivity with Drude model in the interface of two different materials based on the area average algorithm has been introduced into the dispersive FDTD method. Numerical results demonstrate the advantages of our method. We also discuss various issues in scattering characteristic of the plasma array, including the frequency of incident THz waves and separation between each two plasma cylinders.

2. THE DESCRIPTION FOR INHOMOGENEOUS PLASMA CYLINDER ARRAY

For simplicity but without losing its generality, the infinite plasma cylinders have been considered. The incident plane wave is polarized with TM case (E_z, H_x, H_y) in two-dimension (2D) case, where the electric field has a z component only, illuminating as an angle φ_i with respect to the positive x-axis, as shown in Figure 1. Four inhomogeneous plasma cylinders, with radii R_1, R_2, R_3 and R_4, are placed in y-axis, respectively. And d is the separation between each two plasma cylinders.

The inhomogeneous plasma cylinders considered in our work are radially-dependent, and the complex relative permittivity ε with the Drude model is given as follows

$$\begin{aligned}\varepsilon(\omega, r) &= \varepsilon_0 \left(1 - \frac{\omega_p^2(r)}{\omega^2 - j\omega\nu(r)}\right) \\ &= \varepsilon_0 \left(1 - \frac{\omega_p^2(r)}{\omega^2 + \nu^2(r)} - j\frac{\nu(r)}{\omega}\frac{1}{\omega^2 + \nu^2(r)}\right) \end{aligned} \quad (1)$$

where ω is the operating angular frequency, ω_p the plasma frequency, and ν the collision frequency.

Radially-dependent plasma and collision frequency chosen here are similar to the laboratory argon plasma parameters [2] and reentry plasma sheath [1]. It should be pointed out that although the collision frequency is not given in [2], we assume that it also has a radially-dependent profile as the plasma frequency in order to model more

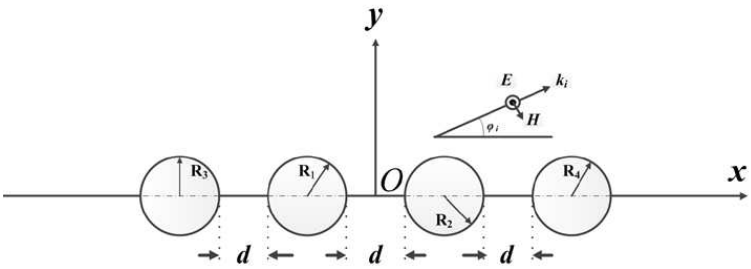

Figure 1. Schematic of simulation model, including four plasma cylinders.

realistic condition. The two parameters are expressed as follows

$$\omega_p(r) = \begin{cases} \omega_{p0}\left(\frac{r}{r_0}\right)^{1/2}, & 0 \le r \le r_0 \\ \omega_{p0}\exp\left(\frac{-(r-r_0)}{2R}\right), & r_0 < r < R \end{cases} \tag{2}$$

$$\nu(r) = \begin{cases} \nu_0\left(\frac{r}{r_0}\right)^{1/2}, & 0 \le r \le r_0 \\ \nu_0\exp\left(\frac{-(r-r_0)}{2R}\right), & r_0 < r < R \end{cases} \tag{3}$$

where ω_{p0} and ν_0 denote the maximum values of plasma and collision frequency, which occur at $r = r_0$, and R represents the radius of a single plasma cylinder. The distributions of ω_p and ν along the radius of the cylinder are shown in Figure 2.

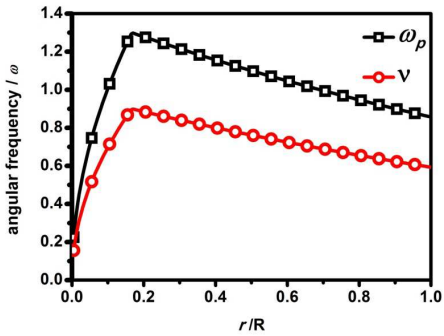

Figure 2. The radially-dependent plasma and collision frequency.

It is a common knowledge that an incident EM wave can propagate in a collisionless plasma above electron plasma frequency $\omega_p/2\pi$. Below $\omega_p/2\pi$, the EM wave cannot propagate into the bulk region and is reflected in a thin evanescent layer on its surface. However, as the plasma become collisional, the EM wave can propagate and attenuate throughout the entire range of ω [6]. By calculation using the formula $\omega_p/2\pi \approx 8.97\sqrt{N_e}\,\mathrm{Hz}$, it can be found that the broadband terahertz wave with the frequency range can transmit through the plasma with electron density range of 10^{20}–$10^{24}\,\mathrm{m}^{-3}$.

Therefore, in this paper, in terahertz wave frequency band, the electron density is assumed to be on the order of 10^{20}–$10^{24}\,\mathrm{m}^{-3}$. The maximum $N_e = 7.9\times10^{20}\,\mathrm{m}^{-3}$ is chosen. The corresponding maximum plasma frequency $\omega_p = 1.58\times10^{12}\,\mathrm{rad/s}$, and the maximum collision frequency $\nu = 1.005\times10^{12}\,\mathrm{Hz}$ is set.

3. THE CONFORMAL DISPERSIVE FDTD METHOD

Among the conformal schemes for modeling dielectric objects as shown in [26, 27], a new equivalent permittivity is introduced to modify the update equations of electric fields. The basic idea of these techniques is that the permittivity of the conformal cells should be determined by an average method with the material information adjacent to the update electric field point. An area weighted permittivity averaging procedure used in the proposed dispersive conformal FDTD method is shown in Figure 3. The interface between FDTD cell and curved surface is depicted in Figure 3(a). In our problem, the interface exists not only in the plasma-vacuum interface, but also in the inside of the inhomogeneous plasma cylinder which is the interface of two dispersive mediums.

At first, we consider the Ampere's law

$$\frac{\partial}{\partial t}\iint_S DdS = \oint_L Hdl \tag{4}$$

$$D = \varepsilon_0 \varepsilon_r E \tag{5}$$

where D is the electric-flux density, H the magnetic field, S the integral surface as the unit cell in Figure 3(b), and L the integral loop along the unit cell.

The locations of E_z and D_z maintain the same as the traditional FDTD method, which samples at the midpoints of a unit cell. Then,

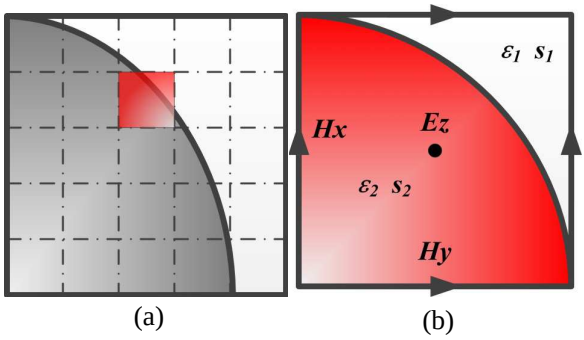

Figure 3. Area weighted permittivity averaging procedure used in proposed dispersive conformal FDTD method. (a) Interface between FDTD cell and a curved surface. (b) Unit cell in the interface treatment technique.

the Ampere's can be discretized in Yee grids in a different form as

$$\begin{aligned}&\iint_S \varepsilon dS \times \left(E_z^{n+1}(i,j) - E_z^n(i,j)\right)\\ &= \begin{bmatrix} \frac{H_y^{n+1/2}(i+1/2,j) - H_y^{n+1/2}(i-1/2,j)}{\Delta x} \\ -\frac{H_x^{n+1/2}(i,j+1/2) - H_x^{n+1/2}(i,j-1/2)}{\Delta y} \end{bmatrix}\end{aligned} \tag{6}$$

Then, the effective permittivity in the conformal cell can be obtained as

$$\begin{aligned}\varepsilon_{eff} &= \frac{1}{S}\iint_S \varepsilon dS = \frac{1}{S}\left(\iint_{S_1} \varepsilon_1 dS + \iint_{S_2} \varepsilon_2 dS\right)\\ &= \frac{S_1(i,j)}{S(i,j)}\varepsilon_1 + \frac{S_2(i,j)}{S(i,j)}\varepsilon_2\end{aligned} \tag{7}$$

where $S_1(i,j)$ and $S_2(i,j)$ are the areas of the inner and outer irregular parts of the unit cell in medium 1 and 2, as shown in Figure 3(b).

Further, substituting the new average effective permittivity in (7) to the constitutive relation in (5), we can get the modified constitutive relation in conformal cells as follows

$$D = \varepsilon_0 \varepsilon_{eff} E = \varepsilon_0 \left(\frac{S_1(i,j)}{S(i,j)}\varepsilon_1 + \frac{S_2(i,j)}{S(i,j)}\varepsilon_2\right) E \tag{8}$$

In order to derive the conformal dispersive algorithm conveniently, the variable r in (1) is omitted. The permittivity of mediums 1 and 2 with Durde model can be given as

$$\varepsilon_i = 1 - \frac{\omega_{pi}^2}{\omega^2 - j\omega\nu_i} \tag{9}$$

where ω_{pi} and ν_i $(i = 1, 2)$ are the plasma and collision frequency in mediums 1 and 2, respectively.

Substituting (9) into (8), after some operation, we can get the average effective permittivity in dispersive medium based on above mentioned conformal technique as

$$\begin{aligned}\varepsilon_{eff} &= \alpha\varepsilon_1 + \beta\varepsilon_2 = \frac{\left(\alpha\omega_{p1}^2 + \beta\omega_{p2}^2\right)\omega - j\left(\alpha\omega_{p1}^2\nu_2 + \beta\omega_{p2}^2\nu_1\right)}{\omega^3 - j(\nu_1+\nu_2)\omega^2 - \nu_1\nu_2\omega}\\ &= \frac{-\left(\alpha\omega_{p1}^2 + \beta\omega_{p2}^2\right)(j\omega)^2 - \left(\alpha\omega_{p1}^2\nu_2 + \beta\omega_{p2}^2\nu_1\right)(j\omega)}{(j\omega)^4 + (\nu_1+\nu_2)(j\omega)^3 + \nu_1\nu_2(j\omega)^2}\\ &= \frac{\sum_{m=0}^{2} p_m (j\omega)^m}{\sum_{m=0}^{4} q_m (j\omega)^m}\end{aligned} \tag{10}$$

where $\alpha = \frac{S_1(i,j)}{S(i,j)}$ and $\beta = \frac{S_2(i,j)}{S(i,j)}$, respectively. And

$$p_0{=}0, \quad p_1 = -\left(\alpha\omega_{p1}^2\nu_2 + \beta\omega_{p2}^2\nu_1\right), \quad p_2 = -\left(\alpha\omega_{p1}^2 + \beta\omega_{p2}^2\right) \tag{11}$$

$$q_0{=}q_1 = 0, \quad q_2 = \nu_1\nu_2, \quad q_3 = (\nu_1 + \nu_2), \quad q_4 = 1 \tag{12}$$

To get the updated equations for dispersive conformal FDTD method, we beginn with the time-domain constitutive relation based on the effective permittivity in (10)

$$D_z(t) = \varepsilon_0\varepsilon_{eff}\left(\frac{\partial}{\partial t}\right)E_z(t) \tag{13}$$

where $\varepsilon_{eff}(\frac{\partial}{\partial t})$ is the expression for permittivity in time-domain.

$$\varepsilon_{eff}\left(\frac{\partial}{\partial t}\right) = \frac{\sum_{m=0}^{2} p_m\left(\frac{\partial}{\partial t}\right)^m}{\sum_{m=0}^{4} q_m\left(\frac{\partial}{\partial t}\right)^m} \tag{14}$$

Substituting (14) into (13), we can get

$$\left[\sum_{m=0}^{4} q_m\left(\frac{\partial}{\partial t}\right)^m\right] D_z(t) = \varepsilon_0\left[\sum_{m=0}^{2} p_m\left(\frac{\partial}{\partial t}\right)^m\right] E_z(t) \tag{15}$$

Next, we consider the temporal discretization form of (15), assuming a function

$$y(t) = \frac{\partial f(t)}{\partial t} \tag{16}$$

The central difference can be approximate by

$$\frac{y^{n+1} + y^n}{2} = \frac{f^{n+1} - f^n}{\Delta t} \tag{17}$$

Introducing the following shift operator

$$z^t f^n = f^{n+1} \tag{18}$$

Combining (17) and (18), we can have

$$y^n = \left(\frac{2}{\Delta t}\frac{z^t - 1}{z^t + 1}\right) f^n \tag{19}$$

Comparing (16) and (19), the following relationship can be obtained

$$\frac{\partial f}{\partial t} \to \frac{2}{\Delta t}\frac{z^t - 1}{z^t + 1} \tag{20}$$

By substituting (20) into (15), the modified constitutive relationship of dispersive time-domain can be given as

$$\left[\sum_{m=0}^{4} q_m \left(\frac{2}{\Delta t}\right)^m \left(z^t+1\right)^{4-m}\left(z^t-1\right)^m\right] D_z^n(i,j) = \varepsilon_0 \left[\sum_{m=0}^{2} p_m \left(\frac{2}{\Delta t}\right)^m \left(z^t+1\right)^{4-m}\left(z^t-1\right)^m\right] E_z^n(i,j) \quad (21)$$

Then, the solution of E_z^{n+1} can be obtained as

$$E_z^{n+1}(i,j) = \frac{1}{b_0}\left[\sum_{m=0}^{4} \frac{a_m}{\varepsilon_0} D_z^{n+1-m}(i,j) - \sum_{m=1}^{4} b_m E_z^{n+1-m}(i,j)\right] \quad (22)$$

where

$$\begin{aligned} a_0 &= q_0 + q_1 u + q_2 u^2 + q_3 u^3 + q_4 u^4 & b_0 &= p_0 + p_1 u + p_2 u^2 \\ a_1 &= 4q_0 + 2q_1 u - 2q_3 u^3 - 4q_4 u^4 & b_1 &= 4p_0 + 2p_1 u \\ a_2 &= 6q_0 - q_2 u^2 + 6q_4 u^4 & b_2 &= 6p_0 - 2p_2 u^2 \\ a_3 &= 4q_0 - 2q_1 u + 2q_3 u^3 - 4q_4 u^4 & b_3 &= 4p_0 - 2p_1 u \\ a_4 &= q_0 - q_1 u + q_2 u^2 - q_3 u^3 + q_4 u^4 & b_4 &= p_0 - p_1 u + p_2 u^2 \end{aligned} \quad (23)$$

where $u = \frac{1}{\Delta t}$, p and q are defined in (11) and (12), respectively.

The updated equation for calculating D_z is

$$D_z^{n+1}(i,j) = D_z^n(i,j) + \frac{1}{\Delta t} \cdot \left[\begin{array}{c} \frac{H_y^{n+1/2}(i+1/2,j) - H_y^{n+1/2}(i-1/2,j)}{\Delta x} \\ -\frac{H_x^{n+1/2}(i,j+1/2) - H_x^{n+1/2}(i,j-1/2)}{\Delta y} \end{array}\right] \quad (24)$$

According to (22) and (24), E_z can be calculated by an $H \to D \to E$ iterative process, and the updated equations for H_x, H_y maintain the same as traditional FDTD method [18].

A near-to-far-field transformation [18] for the FDTD method is needed when calculating the scattered far field E_s^{far}. In 2-D problems, the scattering width σ is defined as

$$\sigma(\phi) = \lim_{r_{far}\to\infty} 2\pi r_{far} \frac{\left|E_s^{far}(\phi)\right|^2}{|E_i|^2} \quad (25)$$

where, ϕ is the scattering angle, r_{far} the distance of the observer point, E_s^{far} the scattered far field, and E_i the incident field.

4. NUMERICAL RESULTS AND DISCUSSION

Based on the above mathematical treatment, numerical computations are carried out so as to verify the accuracy and efficiency of our developed techniques, and investigate the scattering of THz EM waves by inhomogeneous plasma cylinder array described in Section 2. Since there is a lack of analytical solution for the problem, the result calculated by commercial software COMSOL Mutiphysics is used as a benchmark. During the COMSOL Multiphysics simulation, each inhomogeneous plasma cylinder in the array is implemented in a step-wise homogeneous 30 plasma layers approximations.

Firstly, we compare the staircasing FDTD with the proposed method using the same grid step size as $\Delta x = \Delta y = \lambda/30$. The operating frequency of the incident EM wave is $f = 0.2\,\text{THz}$, corresponding to the wavelength in free space $\lambda = 0.15\,\text{m}$. And the incident angle is $\varphi_i = 90°$, and the radii of the four cylinders are $R_1 = R_2 = R_3 = R_4 = 0.5\lambda$, $d = 0.5\lambda$, $r_0 = 0.2R$ as depicted in Figure 1 and 2. The time step is chosen as $\Delta t = \Delta x/2c$ to satisfy the Courant stability condition. The TF/SF boundary condition [18] is used to implement a plane wave source, and 10-cell UPML [18] is used as absorbing boundary condition. The scattering width results from both the staircasing FDTD and the proposed method compared with the benchmark shown in Figure 4(a).

It can be clearly seen that the curve calculated from the proposed method tracing the benchmark better than the counterpart results

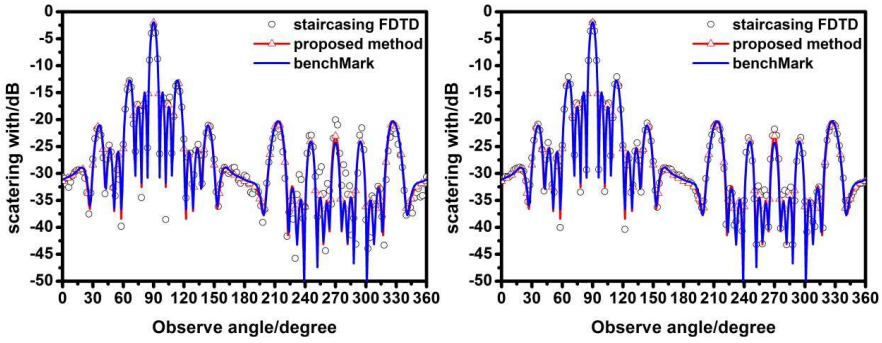

Figure 4. The comparison between proposed method and staircasing FDTD. (a) Both staircasing FDTD and proposed method with $\Delta x = \Delta y = \lambda/30$. (b) Staircasing FDTD with $\Delta x = \Delta y = \lambda/40$, proposed method with $\Delta x = \Delta y = \lambda/30$.

from staircasing FDTD. Figure 4(b) repeats Figure 4(a) with the staircasing FDTD run at $\Delta x = \Delta y = \lambda/40$ instead. Although the spatial-step size of the staircasing FDTD is smaller than the proposed method, the accuracy level is still worse than the proposed method. In order to provide a clearer sight for the accuracy level of the two methods, the global relative two-norm (L_2) error is defined by

$$L_2^{error} = \frac{\int_0^{2\pi} \left\| \sigma(\varphi) - \sigma^{\text{benchmark}}(\varphi) \right\| d\varphi}{\int_0^{2\pi} \sigma^{\text{benchmark}}(\varphi)\, d\varphi} \tag{26}$$

Global relative two-norm errors based on the benchmark of the two methods are shown in Table 1. As shown in the table, the L_2 error of the proposed method is much less than that of the staircasing FDTD, in despite of the latter using smaller spatial step size.

Table 1. The global relative two-norm errors of the two methods.

Method	**spatial step size**	$\boldsymbol{L_2}$ **error**	**CPU time**	**Memory cost**
Staircasing FDTD	$\Delta x = \Delta y = \lambda/30$	1.0898×10^{-2}	145.89 s	40.36 MB
	$\Delta x = \Delta y = \lambda/40$	0.3762×10^{-2}	1137.94 s	286.58 MB
Proposed method	$\Delta x = \Delta y = \lambda/30$	6.1112×10^{-4}	189.66 s	60.54 MB

To solve various practical EM problems, it is very important for us to get balance between accuracy and computational burden. The above numerical example shows that the proposed method is better used to solve this problem. It should be noted that although the proposed method needs two more arrays to store D and E at the previous two time steps in the code, it can reduce the memory cost due to adopting larger spatial step size. As shown in Table 1, regardless of the fact that the proposed method costs more CPU time and memory with the same spatial step size as staircasing FDTD, the L_2 error is much lower than the latter. And when the staircasing FDTD using large spatial-step size, the CPU time and memory cost become much larger than the proposed method.

Next, the scattering characteristic of THz EM waves by inhomogeneous plasma cylinder array with different frequencies and separations is investigated. The spatial-step size used in the proposed method is $\Delta x = \Delta y = \lambda/30$, and the time step is chosen as $\Delta t = \Delta x/2c$.

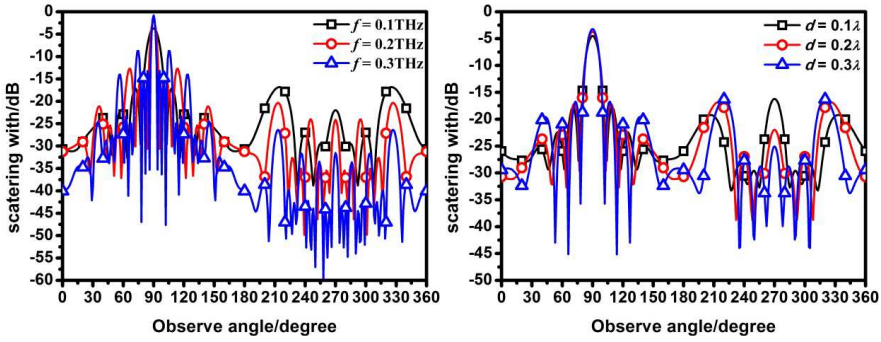

(a) (b)

Figure 5. The scattering width of four plasma array. (a) The separation is $d = 0.2\lambda$ with different frequencies $f = 0.1$, 0.2, 0.3 THz. (b) The frequency $f = 0.1$ THz with different separations $d = 0.1$, 0.2, 0.3λ.

Figures 5(a) and (b) show the far filed scattered width from four plasma cylinders with $f = 0.1$, 0.2, 0.3 THz, $d = 0.2\lambda$ and $f = 0.1$ THz, $d = 0.1$, 0.2, 0.3λ, respectively. The incident EM wave with the angle $\varphi_i = 90^\circ$ hence observing angle $\varphi_s = 90^\circ$ indicates the forward scattering, while $\varphi_s = 270^\circ$ indicates the backward scattering. As can be seen from Figures 5(a) and (b), the forward scattering at point $\varphi_s = 90^\circ$ has only a little difference in spite of the different frequencies and separations, and the scattering width varies markedly with frequency and separation at the other scattered directions. The scattering width curves vary more wildly in angular direction as the frequency becomes higher. The backward scattering becomes weaker as long as the frequency increasing, because the smaller wavelength may enable more EM energy to propagate through the plasma cylinder array. As the separation d increasing, the backward scattering also becomes lower, since wider separation makes the EM energy pass through the plasma array more easily.

Moreover, one of the significant advantages of FDTD method compared to frequency domain method such as COMSOL Mutiphysics involved in EM problems is the time domain EM filed which can be obtained conveniently, thus the EM property in wideband frequency region will be obtained through inverse Fourier transformation. Figure 6 shows the time domain backward far electric field and wideband frequency region RCS. The spatial step size is $\Delta x = \Delta y = \lambda/30$, and the time step is chosen as $\Delta t = \Delta x/2c$. The excitation is Gaussian pulse EM wave $e^i(t) = \exp[-4\pi(t - t_0)^2/\tau^2]$, with $\tau = 60\Delta t$, $t = 0.8\tau$. The incident direction is $\varphi_i = 90^\circ$, and observing direction

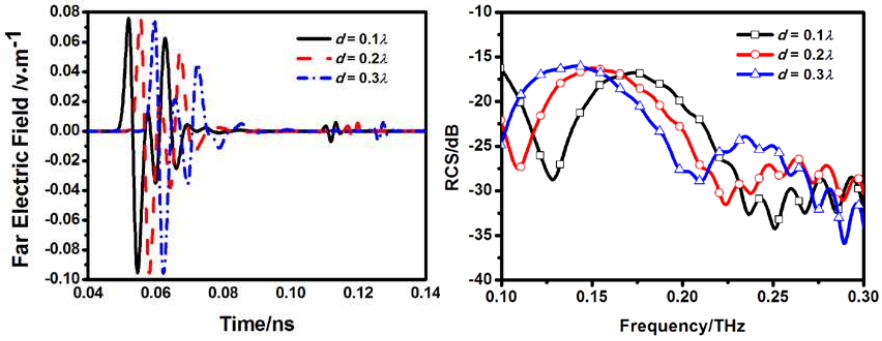

Figure 6. Different separations are $d = 0.1, 0.2, 0.3\lambda$. (a) Time domain backward far electric field. (b) Wideband frequency region RCS.

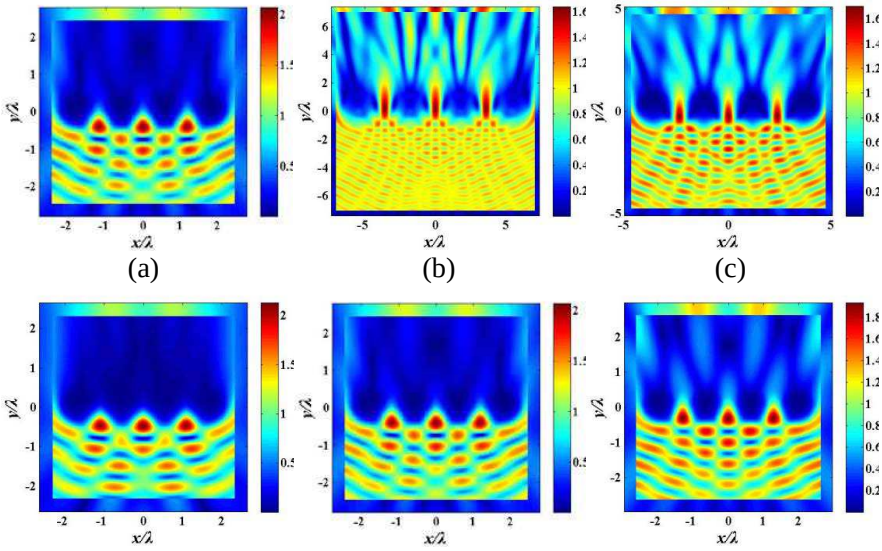

Figure 7. Magnitude of total near electric field E_z. (a) $d = 0.2\lambda$, $f = 0.1$ THz. (b) $d = 0.2\lambda$, $f = 0.2$ THz. (c) $d = 0.2\lambda$, $f = 0.3$ THz. (d) $f = 0.1$ THz, $d = 0.1\lambda$. (e) $f = 0.1$ THz, $d = 0.2\lambda$. (f) $f = 0.1$ THz, $d = 0.3\lambda$.

is $\varphi_s = 270°$.

Finally, in order to demonstrate the scattering characteristic of the plasma array more expressly, the magnitude of total near electric field

E_z is shown in Figure 7, and the TF/SF boundary can be clearly seen in the figure. The EM waves propagate from the bottom to the top of the figure. Figures 7(a)–(c) depict the influence of different frequencies on the near field with the same separation, while Figures 7(d)–(f) depict the influence of different separations on the near field with the same frequency.

From Figures 7(a)–(c), we can find that the magnitude of the total electric field between each two of the four plasma cylinders becomes larger as the frequency increases, and the total electric field distribution in the upper regime becomes wider. In other words, the higher frequency enables more EM energy pass through the plasma array, which will results in weaker backward scattering as shown in Figure 5(a). On the other hand, it can be noted that more EM energy can propagate through the plasma array as the separation becomes larger, depicted in Figures 6(d)–(f), and this is the reason for the smaller backward scattering width as shown in Figure 5(b).

In short, a higher frequency or larger separation enables more EM energy pass through the inhomogeneous plasma cylinder, while the backward scattering width becomes smaller.

5. CONCLUSION

In this paper, in order to reduce the errors resulting from employing the staircase approximation to model curved surface in traditional FDTD method, an area weighted permittivity averaging procedure is used in the proposed dispersive conformal FDTD method. Different from previous works, the proposed method aims to deal with the interface between two dispersive mediums. Numerical results show that the proposed method is superior to the staircase FDTD method when modeling the dispersive medium curved surface. Moreover, the scattering of THz waves by inhomogeneous collisional plasma array is studied. We find that the forward and backward scatterings exhibit different characteristics when the frequency and separation are changed. The research in this paper will be helpful in the field related to the design of intelligent plasma antenna arrays for THz regime and Terahertz telemetry of reentry or hypersonic vehicles through plasma.

ACKNOWLEDGMENT

This work is partly supported by the NSFC under Grant Nos. 61101069 and 61201020, partly supported by the Fundamental Research Funds for the Central University under No. 72114458.

REFERENCES

1. Casey, K., "Radiation through an inhomogeneous reentry plasma layer," *IEEE Transactions on Antennas and Propagation*, Vol. 19, No. 5, 711–712, 1971.
2. Stewart, G., "Laboratory simulation of reentry plasma sheaths," *IEEE Transactions on Antennas and Propagation*, Vol. 15, No. 6, 831–832, 1967.
3. Shi, L., B. Guo, Y. Liu, and J. Li, "Characteristic of plasma sheath channel and its effect on communication," *Progress In Electromagnetics Research*, Vol. 123, 321–336, 2012.
4. Rayner, J. P., A. P. Whichello, and A. D. Cheetham, "Physical characteristics of plasma antennas," *IEEE Transactions on Plasma Science*, Vol. 32, No. 1, 269–281, 2004.
5. Alexeff, I., T. Anderson, S. Parameswaran, E. P. Pradeep, J. Hulloli, and P. Hulloli, "Experimental and theoretical results with plasma antennas," *IEEE Transactions on Plasma Science*, Vol. 34, No. 2, 166–172, 2006.
6. Alexeff, I., T. Anderson, and E. Farshi, "Recent results for plasma antennas," *Physics of Plasmas*, Vol. 15, 057104-4, 2008.
7. Kuz'min, G., I. Minaev, K. Rukhadze, V. Tarakanov, and O. Tikhonevich, "Reflector plasma array antennas," *Journal of Communications Technology and Electronics*, Vol. 57, No. 5, 536–542, 2012.
8. Wu, X. P., J.-M. Shi, Z. S. Chen, and B. Xu, "A new plasma antenna of beam-forming," *Progress In Electromagnetics Research*, Vol. 126, 539–553, 2012.
9. Köhler, R., A. Tredicucci, F. Beltram, H. E. Beere, E. H. Linfield, A. G. Davies, D. A. Ritchie, R. C. Iotti, and F. Rossi, "Terahertz semiconductor-heterostructure laser," *Nature*, Vol. 417, 156–159, 2002.
10. Bartel, T., P. Gaal, K. Reimann, M. Woerner, and T. Elsaesser, "Generation of single-cycle THz transients with high electric-field amplitudes," *Optics Letters*, Vol. 30, No. 20, 2805–2807, 2005.
11. Yang, L., B. Rosam, and M. M. Dignam, "Density-dependent terahertz emission in biased semiconductor superlattices: From Bloch oscillations to plasma oscillations," *Physical Review B*, Vol. 72, 115313, 2005.
12. Liu, J. and X. C. Zhang, "Terahertz-radiation-enhanced emission of fluorescence from gas plasma," *Physical Review Letters*, Vol. 103, No. 23, 235002, Dec. 4, 2009.

13. Jamison, S. P., J. Shen, D. R. Jones, R. C. Issac, B. Ersfeld, D. Clark, and D. A. Jaroszynski, "Plasma characterization with Terahertz time-domain measurements," *Journal of Applied Physics*, Vol. 93, No. 7, 4334–4336, 2003.
14. Yuan, C., Z. Zhou, X. Xiang, H. Sun, and S. Pu, "Propagation of broadband terahertz pulses through a dense-magnetized-collisional-bounded plasma layer," *Physics of Plasmas*, Vol. 17, 113304–113307, 2010.
15. Yuan, C., Z. Zhou, J. W. Zhang, X. Xiang, Y. Feng, and H. Sun, "FDTD analysis of terahertz wave propagation in a high-temperature unmagnetized plasma slab," *IEEE Transactions on Plasma Science*, Vol. 39, No. 7, 1577–1584, 2011.
16. Kim, J. J., D. G. Jang, M. S. Hur, H. Jang, and H. Suk, "Relativistic terahertz pulse generation by non-linear interaction of a high-power fs laser with underdense plasmas," *Journal of Physics D: Applied Physics*, Vol. 45, 395201–395205, 2012.
17. Oh, T. I., Y. S. You, and K. Y. Kim, "Two-dimensional plasma current and optimized terahertz generation in two-color photoionization," *Optics Express*, Vol. 20, No. 18, 19778–19786, 2012.
18. Taflove, A., *Computational Electrodynamics: The Finite-difference Time-domain Method,* Artech House, Norwood, MA, 2000.
19. Wahl, P., D. S. Ly Gagnon, C. Debaes, J. Van Erps, N. Vermeulen, D. A. Miller, and H. Thienpont, "B-calm: An open-source multi-GPU-based 3D-FDTD with multi-pole dispersion for plasmonics," *Progress In Electromagnetics Research*, Vol. 138, 467–478, 2013.
20. Markovich, D. L., K. S. Ladutenko, and P. A. Belov, "Performance of FDTD method CPU implementations for simulation of electromagnetic processes," *Progress In Electromagnetics Research*, Vol. 139, 655–670, 2013.
21. Luebbers, R., F. P. Hunsberger, K. S. Kunz, R. B. Standler, and M. Schneider, "A frequency-dependent finite-difference time-domain formulation for dispersive materials," *IEEE Transactions on Electromagnetic Compatibility*, Vol. 32, No. 3, 222–227, 1990.
22. Sullivan, D. M., "Frequency-dependent FDTD methods using Z transforms," *IEEE Transactions on Antennas and Propagation*, Vol. 40, No. 10, 1223–1230, 1992.
23. Gandhi, O. P., B. Q. Gao, and J. Y. Chen, "A frequency-dependent finite-difference time-domain formulation for general dispersive media," *IEEE Transactions on Microwave Theory and Techniques*, Vol. 41, No. 4, 658–665, 1993.

24. Hulse, C. and A. Knoesen, "Dispersive models for the finite-difference time-domain method: Design, analysis, and implementation," *Journal of the Optical Society of America A (Optics and Image Science)*, Vol. 11, No. 6, 1802–1811, 1994.
25. Chun, K., H. Kim, H. Kim, and Y. Chung, "PLRC and ADE implementations of drude-critical point dispersive model for the FDTD method," *Progress In Electromagnetics Research*, Vol. 135, 373–390, 2013.
26. Kaneda, N., B. Houshmand, and T. Itoh, "FDTD analysis of dielectric resonators with curved surfaces," *IEEE Transactions on Microwave Theory and Techniques*, Vol. 45, No. 9, 1645–1649, 1997.
27. Supriyo, D. and R. Mittra, "A conformal finite-difference time-domain technique for modeling cylindrical dielectric resonators," *IEEE Transactions on Microwave Theory and Techniques*, Vol. 47, No. 9, 1737–1739, 1999.
28. Yu, W. H. and R. Mittra, "A conformal finite difference time domain technique for modeling curved dielectric surfaces," *IEEE Microwave and Wireless Components Letters*, Vol. 11, No. 1, 25–27, Jan. 2001.
29. Wang, J., W. Yin, P. Liu, and Q. Liu, "High-order interface treatment techniques for modeling curved dielectric objects," *IEEE Transactions on Antennas and Propagation*, Vol. 58, No. 9, 2946–2953, 2010.
30. Kong, L.-Y., J. Wang, and W.-Y. Yin, "A novel dielectric conformal FDTD method for computing SAR distribution of the human body in a metallic cabin illuminated by an intentional electromagnetic pulse (IEMP)," *Progress In Electromagnetics Research*, Vol. 126, 355–373, 2012.
31. Mohammadi, A., H. Nadgaran, and M. Agio, "Contour-path effective permittivities for the two-dimensional finite-difference time-domain method," *Optics Express*, Vol. 13, No. 25, 10367–10381, 2005.
32. Mohammadi, A. and M. Agio, "Dispersive contour-path finite-difference time-domain algorithm for modelling surface plasmon polaritons at flat interfaces," *Optics Express*, Vol. 14, No. 23, 11330–11338, 2006.
33. Mohammadi, A., T. Jalali, and M. Agio, "Dispersive contour-path algorithm for the two-dimensional finite-difference time-domain method," *Optics Express*, Vol. 16, No. 10, 7397–7406, 2008.